Rubidium localization in single-walled carbon nanotube bundles: Structural study

N. Bendiab*
Institut Néel, Université Joseph Fourier et CNRS, 34020 Grenoble, France

A. M. Saitta
Institut de Minéralogie et de Physique des Milieux Condensés, CNRS-UMR 7590, Université Pierre et Marie Curie-Paris 6, Université Denis Diderot-Paris 7, IPGP, F-75252 Paris, France

R. Aznar, J. L. Sauvajol, and R. Almairac
Laboratoire des Colloïdes Verres et Nanomatériaux, CNRS-UMR 5587, Université Montpellier II, 34095 Montpellier Cedex 5, France

I. Mirebeau and G. Andre
Laboratoire Léon Brillouin, CEA et CNRS, 91191 Gif-sur-Yvette, France

(Received 12 February 2008; revised manuscript received 27 June 2008; published 15 September 2008)

X-ray and neutron-diffraction investigations of rubidium-intercalated single-walled carbon nanotubes are reported. *Ab initio* calculations conducted in combination with our experiments show that for a single Rb ion the most energetically favorable intercalation site is the interstitial channel between three tubes in a bundle. At higher doping levels, as the Rb content increases, this site becomes however unfavored with respect to the interior of the tubes or the external surface of the bundle. Model simulations of the diffraction patterns, capable of well reproducing both the x-ray and neutron-diffraction patterns, indicate that only the latter insertion sites are compatible with the experimental data. Finally we show that the bundle surface site is the most probable one in the case of saturation at an estimated stoichiometry close to RbC_8.

DOI: 10.1103/PhysRevB.78.104108 PACS number(s): 61.46.Fg, 71.15.Mb, 61.05.cp, 61.05.fm

I. INTRODUCTION

Single-walled carbon nanotubes (SWNTs) constitute, due to their unique structural and electronic properties, a new class of materials of great interest in the development of novel nanoscale electronic devices. The tunability of their electronic properties by controlling their Fermi level is major issue in such device applications; as a consequence, the understanding of their structural and electronic properties under doping is of crucial importance. Recently, a significant amount of experimental and theoretical work on their electronic properties have shown the effective possibility of tuning their Fermi level by electron or hole doping using acceptor or donor intercalation[1–13] or by applying a gate voltage.[14–18] Experiments show that the maximum intercalation ratio C/M (alkali metals) is $\sim 8:1$ as for the highest doping level in graphite but the localization of these dopants inside the nanotube bundle is not yet solved.

In a bulk sample, most of the single-walled carbon nanotubes are organized in a two-dimensional (2D) triangular lattice of finite size forming long crystalline bundles. These bundles of SWNTs present various cavities that can be filled with molecules or ions. Molecular-dynamics simulations have shown that gas molecules can occupy different sites inside the bundle: the so-called "groove" (G), in between two adjacent tubes at the outer surface of the bundle (GS), the interstitial channel (T) in the triangular void in between three tubes, the exterior surface of the bundle (S), and the inner hollow cavity of the tubes (I). These sites can be differently occupied according to the chemical nature and the size of the guest species.

The 2D triangular lattice is featured by a (10) Bragg peak at 0.4 $Å^{-1}$ in the x-ray and neutron-diffraction diagrams of usual SWNT samples.[19,20] X-rays diffraction has shown a Q downshift of the (10) Bragg peak in alkali-doped SWNT bundles.[21,22] This observation has been generally described in terms of a 2D lattice expansion, and different models of arrangement of the alkali atoms in doped SWNT bundles have been proposed to explain it. In close-end SWNTs, the dopants are expected to be inserted into the interstitial channel (T) between the adjacent SWNTs according to a continuous model[22] and to *ab initio* calculations.[23] In these two models, the insertion of alkali ions in the interstitial channels requires a significant expansion of the triangular lattice.

In this paper, we present combined x-ray and neutron-diffraction investigations, performed on the same alkali-doped SWNT sample, which question the relation between the expansion of the lattice and the position of the (10) Bragg peak in alkali-doped SWNT. We also compare these experimental results to *ab initio* calculations and to a diffraction model. We conclude that the most probable site occupied by the alkali atoms is the bundle surface, i.e., in the present case the Rb atoms do not penetrate inside the SWNT bundles.

II. EXPERIMENTAL SETUP

The nanotube sample was synthesized by the electric arc method using a mixture of nickel and yttrium as catalysts $\sim 99:0.5:0.5\%$ at. of C:Ni:Y. In this case the raw material was made of a large collection of soft cottonlike parts, which have been characterized by x-ray diffraction and selected according to the strength of the (10) Bragg reflection of the bundles. Consequently, the sample we studied contained a large amount of bundles. The powder was separated into two parts, one as reference materials (called "pristine" or "raw")

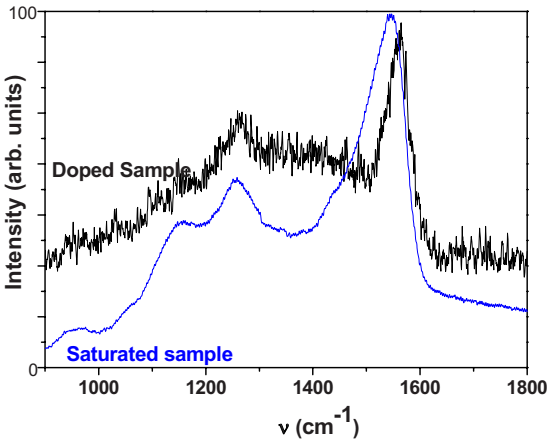

FIG. 1. (Color online) Comparison of saturated Raman spectra (in blue) and present inserted sample Raman spectra.

and the other was used for Rb insertion. In this selected part, the tube diameters are estimated to be about 1.4 ± 0.2 nm. After outgassing and annealing the powder at 250 °C for 48 h under dynamical vacuum, doping of SWNT bundles in the vapor phase was achieved in a Pyrex reactor by heating rubidium metal at 180 °C. A difference of temperature of about 20 °C was imposed between the alkali-metal reservoir and the SWNT sample in order to prevent alkali-metal condensation on the sample. The sample was exposed to rubidium vapor phase during 12 h. The estimated stoichiometry is $RbC_{9\pm1}$ (saturated phase). The nanotube sample was characterized before and after the intercalation process by measuring its Raman and its x-ray and neutron-diffraction diagrams.

X-ray data were collected using a curve position sensitive detector INEL-CPS 120 equipped with a Cu $K\alpha$ (1.542 Å) source and a Ge monochromator. Neutrons data were measured on the G6-1 and G4-1 diffractometers at the Laboratoire Léon Brillouin in Saclay with 4.741 and 2.4266 Å incident wavelengths, respectively. A banana-type detector covering a 80° 2θ range were used with two positions so that a 150° 2θ range could be explored. The neutron-diffraction data were collected for the sample using a mass of 50 mg, whereas the x-ray data were obtained on a smaller mass of about 1 mg.

III. EXPERIMENTAL RESULTS

A. Raman results

First, in order to have a reasonable estimate of the sample stoichiometry, we compared the Raman spectra of the inserted sample to a saturated-doped sample. From the similarity of the spectra, we can argue this sample is a quasisaturated one (see Fig. 1), and its stoichiometry can be estimated as (close to) RbC_8. Once the preliminary Raman study was achieved, we performed x-ray and neutron-diffraction experiments to determine their structure and the localization of the rubidium atoms.

B. Diffraction

In Fig. 2 we present the x-ray and neutron-diffraction patterns for the reference sample and for the intercalated powder. As expected the raw sample displays the same diffraction pattern in both cases. The simulated pattern of raw material is found to be in good agreement with the data and thus provides the structural characteristics of the raw sample, such as the mean tube diameter of 13.6 Å with a cell parameter of 16.7 Å and a diameter distribution of 2 Å (Gaussian distribution assumed). The diffraction model calculations were performed for bundles containing 30 tubes.

Upon rubidium intercalation, the x-ray-diffraction pattern changes (see Fig. 2). The (hk) reflections of the bundles arise above a large background (see the horizontal line which indicates the zero level), probably due to some structural disorder. One observes a strong shift of the (10) peak to small Q and a decrease in its intensity, in contrast with the neutron-diffraction pattern which shows no shift of the (10) peak. This large discrepancy between the x-ray and neutron-diffraction patterns is thus an unexpected result requiring further investigation. The downshift of the (10) peak would reflect a 13% apparent increase in the cell parameter of the bundles in the usual approach. One would logically conclude that the intercalation of the rubidium atoms occurs in be-

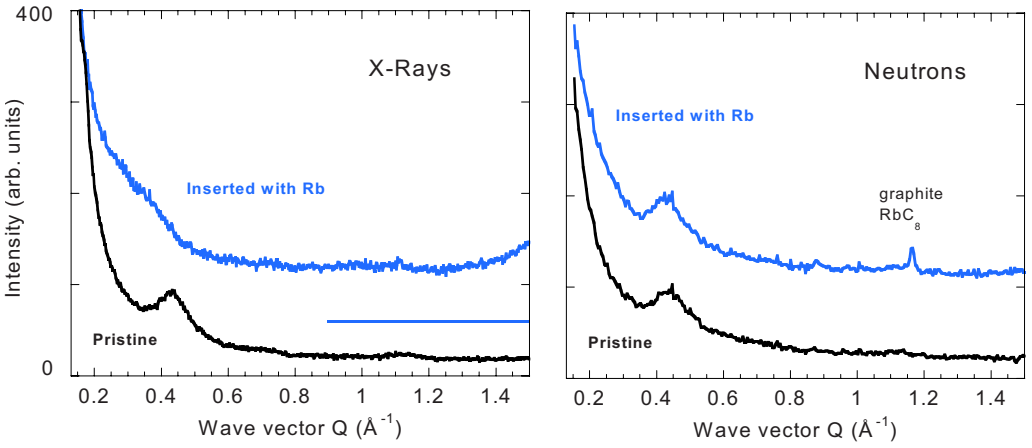

FIG. 2. (Color online) X-ray and neutron-diffraction patterns before and after intercalation. X ray: the horizontal line indicates the zero level for the inserted sample.

TABLE I. Comparison of the respective contributions of rubidium and carbon to the total response obtained with both radiations.

	Source	Rb	C	Crossed
RbC_8	X rays	20%	31%	49%
	neutrons	1.4%	78%	20.6%

tween the tubes (T sites) resulting in a strong increase in the apparent tube-tube distance inside the bundles. This hypothesis has been supported by other groups in the case of SWNT bundle intercalation.

However, when considering the neutron data this interpretation of the x-ray pattern should be questioned. A careful inspection of the other (*hk*) reflections of the triangular lattice could give precise information on the parameter expansion. The other reflections are well defined in the x-ray patterns of the pure compounds (see Fig. 2) but they are very weak in the intercalated ones, this might reflect the partial disordering of the bundles after intercalation. A first insight on the origin of the difference in between the position of the (10) peak into the neutron and x-ray diagrams can be obtained by comparing the respective contributions of rubidium and carbon to the total response obtained with both radiations (Table I). This can be done by comparing the scattering factors (x ray) and the scattering amplitudes (neutrons) for both elements (response at $Q=0$).

The first column represents the weight associated to the contribution of the rubidium structure, the second column represents the weight associated to the tubes contribution, and the last column represents the weight affected to the crossed interference reflecting the relative position of the tubes and rubidium atoms. Taking the neutrons response of RbC_8 as an example, the contribution of rubidium to the total response is 1.4%, of carbon tubes is 78%, and the contribution of the crossed term is 20.6%. The neutrons are therefore more sensitive to the nanotubes response. As the change in the (10) peak position is negligible for neutrons, the effect of rubidium intercalation inside the bundle structure should not be interpreted as an expansion of the tube-tube distance. The direct consequence of this observation is that the (10) shift observed in x-ray diffraction pattern is very unlikely due to a lattice expansion and then its origin should be searched elsewhere. The origin of this shift is clearly the participation of the rubidium atoms to the global response. As it was described in a previous work,[21] the diffraction response of doped samples is subtle and determined by a competition between the contribution of the structure factor and of the form factor. This competition gives unexpected effects. The explanation of this apparent contradiction between x rays and neutron pattern has to be found in respective weight of these contributions, whose role can be obtained by calculating the exact response of SWNT bundles. The insertion of one rubidium ion in the *T* site is easily achieved as in principle it only needs a 0.8% expansion of the triangular lattice but when the number of rubidium dopants increases the expansion necessary to accommodate the intercalating atoms becomes too large to be compatible with the neutron pattern. To obtain quantitative indications about the occupation sites of the rubidium ions, we performed *ab initio* calculations. Moreover, we developed a numerical diffraction model in order to interpret the experimental diffraction patterns.

IV. *AB INITIO* CALCULATIONS

A. Computational details

The combination of accurate experimental spectra, from both neutron and x-ray scattering experiments, and of a model for the interpretation of such spectra gives us precious insights on the localization of Rb intercalants in nanotube bundles. Other important pieces of information can be obtained through *ab initio* calculations. Our first-principles calculations are based on density-functional theory (DFT) within the plane-wave (PW)/pseudopotential scheme implemented in the QUANTUM-ESPRESSO code.[24] We adopt a Perdew-Burke-Erzherhof gradient-corrected functional and ultrasoft pseudopotentials to describe the C and Rb atoms. A PW kinetic-energy cutoff of 30 Ry is sufficient to ensure convergence on the structural, electronic, and vibrational properties. We study the (9,9) metallic armchair SWNT, whose unit cell contains 36 distinct carbon atoms and whose tube diameter is 12.3 Å. Although smaller than the average experimental diameter, this value falls within the experimental size distribution. On the other hand, it allows a significant reduction in computer-time demand. Calculations with six Rb dopants occupying the GT sites were repeated with a (10,10) nanotube having a diameter of 13.6 Å. Integrations in the nanotube one-dimensional Brillouin zone have been performed by using regular grids of **k** points along the **c** reciprocal axis. We use a Fermi-Dirac electronic smearing of 0.01 Ry, and grids of 8**k** points were sufficient to ensure convergence.

The structural calculations are performed by setting the nanotube in an infinite lattice of hexagonal symmetry in the plane perpendicular to the tube axis *z*, mimicking thus the bulk effect of a real nanotube bundle or an isolated tube by varying the intertube distance d_{IT}, whose experimental estimate is $d^{expt} \approx 3.1$ Å. We note here that the use of periodic boundary conditions only allows the study of the T, GT (grooves in triangular site), and I intercalation sites, while the GS and S (surface) site would necessitate a much larger system, too expensive from the computational point of view. However, although no explicit calculations have been carried out for the surface sites, the results for the other intercalation sites allow a reliable prediction, as we will show in the following. Our simulation box contains three unit cells along the *z* direction, and thus 108 carbon atoms; the *c* side of the hexagonal box equals thus 7.38 Å and is maintained constant throughout the calculations. This distance is sufficient to minimize the interaction of the Rb dopants with their periodic images. The choice of only two unit cells along the *z* direction, which would significantly reduce the computational cost, is unfeasible since it would imply each rubidium atom to be at a distance of only 4.92 Å, very similar to typical Rb-Rb distances, from its periodic images. In other words, given the periodic boundary conditions, each rubidium atom in the calculation box would correspond to ac-

tually describing an infinite Rb chain rather than an individual atom, which would certainly alter its electronic and chemical properties.

B. Geometry of the intercalation

An accurate study of the geometrical aspects of the intercalation is necessary to the choice of the most probable doping configurations. We will see in the following that this analysis leads to a substantial difference in the geometry of the intercalation whether it occurs inside (I sites) or outside (T and/or GT sites) the tubes. On the other hand, the surface (GS sites) intercalation is likely independent of the geometry, the energetics playing the major role. Since we are mainly interested in the possible expansion of the nanotube lattice, we focus first on the geometry of the hexagonal base of the unit cell of parameter $a=15.7$ Å, and then on the vertical direction, parallel to the **c** axis. We can define an effective thickness d_{NT} of the nanotube wall as twice the minimum distance beyond which outer atoms (including the walls of other nanotubes) cannot approach. This quantity helps in the estimate of the surface areas, perpendicular to the tube axis, actually available to the dopants; a reasonable choice for d_{NT} is the experimental intertube distance d^{expt}. Indicating with d the diameter of the nanotube and with d_{IT} the intertube distance, the total base area of the unit cell is

$$A_{\mathrm{cell}} = a^2\sqrt{3}/2 \approx 213 \ \text{Å}^2 \tag{1}$$

in our unexpanded (9,9) SWNT case, where $d_{\mathrm{IT}}=d^{\mathrm{expt}}$. Please note that however $d_{\mathrm{IT}} > d_{\mathrm{NT}}=d^{\mathrm{expt}}$ for expanded lattices, as schematically shown in the top panel of Fig. 3. Considering that the typical Rb-C distance is $d^{\mathrm{Rb\text{-}C}}=3.2$ Å, an individual rubidium close to a nanotube wall occupies an area

$$A^{\mathrm{RbC}} = (d^{\mathrm{Rb\text{-}C}} - d_{\mathrm{NT}}/2)^2\pi \approx 7 \ \text{Å}^2. \tag{2}$$

Since the typical Rb-Rb distance is $d^{\mathrm{Rb\text{-}Rb}}=4.9$ Å, as inferred not only by bulk rubidium but also by the graphitic RbC_8 intercalated compound, we can argue that when two or more rubidium atoms occupy the same portion of space, its effective radius can be estimated as $\sqrt[3]{((d^{\mathrm{Rb\text{-}C}}-d_{\mathrm{NT}}/2)^2 d^{\mathrm{Rb\text{-}Rb}})}$, and the effective area per rubidium atom as $A^{\mathrm{Rb}} \approx 15$ Å^2.

In the I-site intercalation, the area available to the dopants depends of course on the individual diameter of each of the nanotubes in the bundles: $A^{\mathrm{I}}_{\mathrm{NT}}=(d-d_{\mathrm{NT}})^2\pi/4$. Given that realistic SWNTs, such as those present in our experimental samples, have diameters larger than 12 Å, the circular-shaped area available to the rubidium atoms is at least 58 Å^2, and it equals 63 Å^2 in the (9,9) SWNT case. In the outside intercalation cases (T and GT sites), the available area per unit cell, A_{free}, is given by the difference of the total area of the unit cell, A_{cell}, and the area of the outer nanotube section, $A^{\mathrm{O}}_{\mathrm{NT}}=(d+d_{\mathrm{NT}})^2\pi/4=193$ Å^2. A_{free} is essentially determined by the intertube distance, and with our structural parameters it equals 20 Å^2. However, it should be noted that it consists of two almost-disconnected quasitriangular portions, which reduces the total available area into two areas of 10 Å^2 each. An increase in the intertube distance d_{IT} of about 1.5 Å (+9% of the lattice parameter) is necessary in order to increase the area of each triangular intertube portion ($A_{\mathrm{free}}/2$) to about 30 Å^2 and thus to accommodate two rubidium atoms.

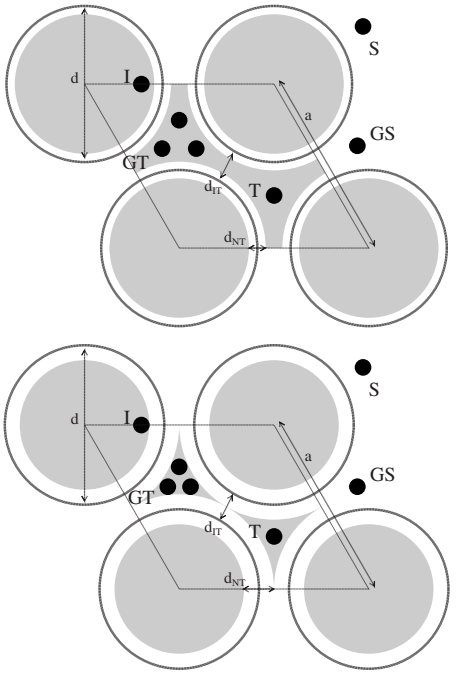

FIG. 3. Schematic representation of the possible intercalation sites in a nanotube bundle. The different sites and distance are labeled according to the text. The gray-shaded areas indicate the region that can actually be occupied by the Rb intercalants at the (undoped) equilibrium lattice parameter (bottom panel) or in the case of lattice expansion (top panel).

In the study of the geometry in the vertical direction, one should note that the use of a periodicity commensurate to the geometry of the carbon nanotube somehow "forces" rubidium atoms to be farther from each other along the vertical direction than 7.38 Å. However, in real samples the local organization of the dopants is not constrained to be commensurate to the nanotube. As a consequence, an arrangement of the Rb atoms locally stable in our calculation box could probably be further "compressed" along the tube axis in real samples. We conclude that the doping ratios corresponding to our calculated local structures of the intercalated atoms might be up to 35% larger in experimental samples, depending on the specific geometry.

The conclusion of this preliminary analysis of the geometry of doping is that only two Rb atoms per unit cell might occupy the T sites outside the tubes. This configuration corresponds to a theoretical (experimental) doping ratio of $\sim$50 ($\sim$35), i.e., RbC_{50} (RbC_{35}). Higher outside dopant concentrations can be achieved only by occupying the GT sites but likely at the expense of a large lattice expansion. On the other hand, the I sites inside the tubes are likely to easily accommodate a larger number of Rb atoms.

C. Results

1. Preliminary steps: Isolated tube

The first step of our first-principles calculations is the study of the undoped nanotube. Our calculated nanotube di-

ameter is very close to the experimental value. The theoretical determination of the ideal lattice parameter is however quite difficult since the potential energy is almost flat as a function of the lattice parameter around the equilibrium value; we observe a very shallow minimum, for the (9,9) SWNT, at about 16.7 Å, i.e., about 1 Å or 6% larger than the 15.7 Å experimental data. We ascribe this discrepancy to the gradient corrections that, contrary to the local-density approximation, tend to predict too weak nonbonded interactions. Given this very weak dependence of the energy from the lattice parameter, we chose to study the different intercalated systems at different fixed lattice parameters, rather than relaxing it along with the structural optimization of any given configuration.

Another preliminary step of our computational approach consisted in the determination of the optimal localization site of a single Rb atom, which corresponds to a theoretical C/Rb doping ratio of ~100, on both the external and internal walls of an isolated tube. To this end, we chose a hexagonal lattice parameter of 26.5 Å, which corresponds to an intertube distance of about 14 Å. In both the external and the internal case, the Rb atom tend to localize close to the center of a carbon hexagon, such that the average distance with its 6 closest carbon neighbors is about 3.2 Å. This result is in excellent agreement with the extended x-ray absorption fine-structure (EXAFS) data of Bantignies *et al.*[25] The adsorption energy, calculated as the difference between the energy of the system when the rubidium is very far away from the SWNT and the energy when it locates at the optimal distance from the (internal or external) tube wall, is about −0.8 eV.

2. Calculations on bundles: One intercalated atom

Once the lattice parameter is fixed to the experimental value of 15.7 Å and the system mimics thus an infinite bundle of identical (9,9) SWNTs, we find that the optimal localization of an individual Rb dopant is very close to the T site with an adsorption energy of about −1.9 eV. This arrangement should not induce any lattice dilatation since the dopant is at an average distance of about 3.2 Å from the tube walls. However, it would induce a significant increase in the intensity of the (10) peak, in contrast with the experimental results.

In the case of an individual rubidium atom localized by the internal wall of the nanotube (I site), the absorption energy is very similar to the case of the isolated tube, about −0.8 eV. Its main effect on the x-ray spectrum is a decrease in the intensity of the (10) line, which agrees with experiments. The intercalation energy in the case of GS-site adsorption, which should not induce significant variations of the lattice parameter, can be estimated around −1.5 eV. In other words, the T site is the most favorable insertion site in terms of the energetics, the more since it should not induce any significant variation of the lattice parameter, but it is not compatible with the observed decrease in the (10) peak. We note that in real experimental systems, this intercalation configuration imply that Rb atoms must lie more or less parallel to the nanotube axis; as a consequence, their respective distance will be around 4.9 Å, i.e., significantly smaller than our imposed periodicity and the resulting experimental doping ratio in the same configuration probably as low as 70.

3. T-site intercalation with two or more atoms

The insertion of more than a single rubidium atom in the system requires a careful analysis of the possible distribution of the dopants with respect to the triangular arrangement of the nanotubes in the bundle. In particular, since there are two T sites per cell unit, a second Rb atom (theoretical/experimental doping ratio ~50/~35, see above) would likely occupy the second one. In this case, the calculated adsorption energy per atom is about −1.7 eV, and the lattice parameter increases in a small amount (1%). The intercalation of two rubidium dopants between the nanotubes is also possible when the atoms occupy two groove (GT) sites within the same triangular T cavity. This configuration is however unstable unless accompanied by a significant increase in the lattice parameter, of the order of 10%, as predicted by the geometrical analysis. Even in that case, the adsorption energy per atom would be slightly smaller (about −1.55 eV) than the intercalation in the two T sites. The energy of the adsorption of two Rb atoms inside a nanotube (I sites) would be significantly smaller (in absolute values), about −0.9 eV per atom. The surface intercalation energy at low doping levels should vary only negligibly since rubidium atoms are likely to be adsorbed at different sites on the surface and thus to have little or no interaction at all.

The insertion of three or more rubidium atoms between the nanotubes necessarily implies that at least two of them must occupy the same triangular T cavity and thus be stable only in the presence of a large lattice parameter increase. In this regard, particularly interesting is the case of doping with six Rb atoms, corresponding to a theoretical (experimental) C/Rb doping ratio of 18 (~14), which represents a sort of geometrical limit for "simple" intercalation external to the nanotubes. Those six intercalants can in fact be placed in the six GT sites of the two triangular cavities. Beyond this limit, a significant structural reorganization and a major lattice expansion (>15%) are required for the system to be stable.[26] We carried out calculations on the Rb_6C_{108} system by placing the six alkali atoms between (GT sites) or inside (I sites) the nanotubes. In the former case, the atoms were put at the six GT sites and different heights $(\frac{1}{3}c, \frac{2}{3}c, c)$. In the unexpanded lattice this configuration is highly unstable and did not even converge to an energy value. Once we allow a lattice relaxation of 11.5%, the system is relaxed and brought to structural equilibrium; the corresponding adsorption energy per dopant is about −1.25 eV. However, the corresponding (10) peak intensity is almost doubled with respect to the undoped case. Very similar results were found in a test with a slightly larger (10,10) nanotube.

4. I-site intercalation with two or more atoms

In the case of I doping the system, independent of the initial configuration, evolves along the relaxation such that at the end the six Rb atoms are located roughly on two different levels along the c direction, one with four atoms and the other one with two atoms. The adsorption energy per Rb

atom is about −0.9 eV, which is slightly more negative than in the case of the I-site adsorption of a single Rb atom. This indicates that the system can favorably accommodate more dopants. In fact, we observe that in order to maximize the interaction of the positively charged rubidium dopants with the negatively charged nanotube walls and to optimize the mutual Rb-Rb distance, the most favorable arrangement in the (9,9) SWNT is the one in which four rubidium atoms are roughly on the same plane. This is actually in good agreement with the geometrical analysis, which predicted an inner available area A_{NT}^{I} of about 63 Å^2 and an effective area per rubidium atom $A^{\mathrm{Rb}}=15$ Å^2, i.e., $A_{\mathrm{NT}}^{\mathrm{I}} \approx 4A^{\mathrm{Rb}}$. In fact, our calculations show that the inclusion of two more rubidium dopants in the plane containing only two atoms, corresponding to a doping ratio of 12, occurs with no significant decrease in the adsorption energy per atom (−0.85 eV). In both cases (six or eight I-site dopants) the (10) line intensity drops dramatically.

5. Extrapolation to surface intercalation

The estimate of the adsorption energy in the case of GS-surface intercalation is more difficult for higher doping concentrations since dopants are denser and denser at the surface, and their interaction becomes more and more important. However, in the case of internal (I-site) doping with two Rb atoms we observed that the energy is lower when they are at a distance of about 4.9 Å, rather than farther apart. Moreover, since no strong geometrical constraints are present at the surface, we can conclude that the adsorption energy per atom might still be of the order of −1.5 eV, thus making the bundle surface the more likely intercalation sites. The conclusions of our first-principles study are that at saturation (~8) the GT (intertube)-doping energy is likely to be even worse than −1.25 eV since larger and larger bundle lattice expansion would be required. Moreover, these configurations are incompatible with the strong decrease in the (10) peak, observed experimentally in the x-ray spectra. On the other hand, the I-site doping does not require a lattice expansion, and the results at fixed lattice parameter indicate that these configurations are more stable and compatible with saturation doping, but their energetics is still unfavorable with the (likely) adsorption energies of the surface intercalation. To go further, we also perform a numerical model to calculate the diffraction pattern for the different configurations.

V. SIMULATIONS OF THE DIFFRACTION PATTERNS

In this section we present calculations of the diffraction pattern for different configurations of SWNT bundles inserted by rubidium ions. Using a numerical model, we can investigate the different possible insertion sites and compare their specific diffraction patterns to the experimental ones.

A. Model description

A real sample of SWNT is made of bundles with different sizes and different tube diameters. Accordingly we consider a collection of seven bundles with different sizes ranging from a small bundle of three tubes to a bundle of 19 tubes (Figs. 4 and 5). The calculated intensity $I(Q)$ diagram is obtained by averaging the seven $I_n(Q)$ curves of each bundle with a Gaussian distribution function centered on the fourth case. The method used to calculate the $I_n(Q)$ intensity curve of a bundle has been described elsewhere.[20,21] $I_n(Q)$ is simply the space average of the square modulus of the amplitude $A_n(\vec{Q})$, where $A_n(\vec{Q})$ stands for the Fourier transform of the collection of atoms considered, i.e., the bundle plus the Rb^+ ions. Presumably the proportion of small bundles in a real sample is larger than that of large ones. For this reason we divided the seven $I_n(Q)$ curves by the number of tubes in each bundle before applying the distribution function. Moreover the tube diameter dispersion is accounted for by averaging the intensity curves $I(Q)$ with a Gaussian distribution function centered on the mean tube diameter determined for the raw sample.

FIG. 4. (Color online) The collection of bundles used for model calculations. Bundles of 3, 6, 7, 12, 13, 18, and 19 tubes. The sixth bundle is shown in Fig. 5. The different sites occupied by Rb^+ ions are shown in the figure. From left to right: raw, grooves (GS), triangular channels (t), interior (i) random, interior (i) surface, and grooves (GS).

For simplicity we assume a uniform scatterer distribution of carbon atoms on the cylindrical surface of each tube. In contrast the rubidium ions inserted inside the bundles are considered individually. Their positions are either ordered or randomly distributed in the occupied site. This assumption obliges to consider tubes of finite length, which we chose equal to 45 Å. This small tube is repeated along the tube axis so as to get a final tube length of ~1000 Å which is the length used for the simulation. The diffraction patterns were calculated in the following cases (see Figs. 4 and 5):

(a) raw SWNT;
(b) Rb in the triangular channels (T);
(c) Rb in the grooves of the triangular channels (GT);
(d) Rb inside tubes close to the interior surface (I) according to *ab initio* predictions;
(e) Rb in grooves at the exterior bundle surface (GS); and
(f) Rb at the bundle surface (as in Fig. 5—one or more layers) (S).

It is clear from Sec. IV and from Figs. 4 and 5 that the Rb content in a bundle is strongly dependent on the possible

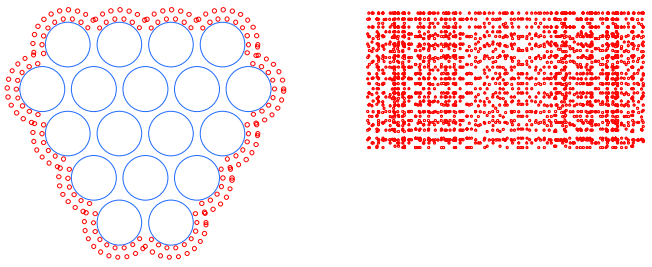

FIG. 5. (Color online) The sixth bundle. The occupied site is the exterior surface of the bundle with two layers (S). Right: view of the Rb^+ ions along the tube axis (projection).

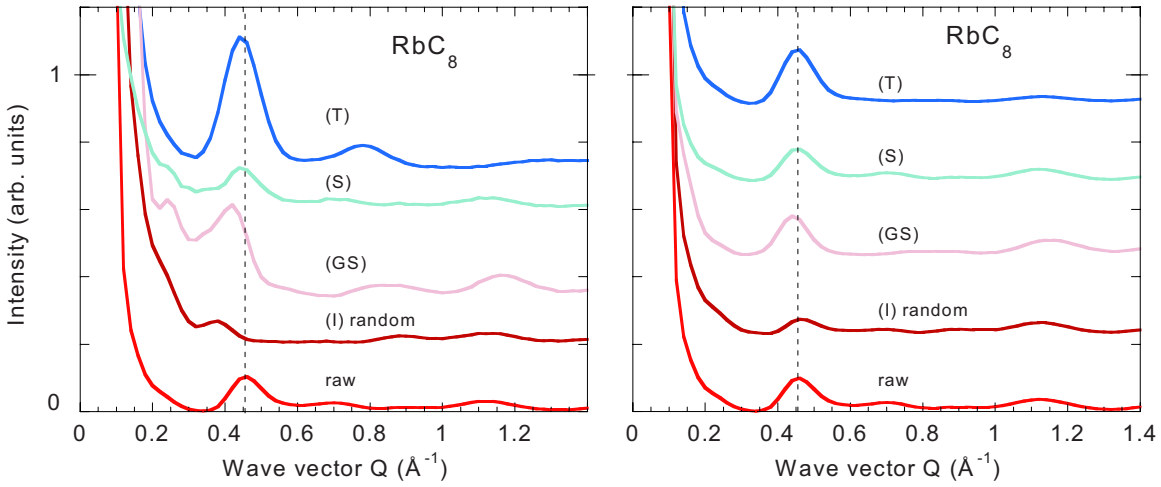

FIG. 6. (Color online) Diffraction patterns simulated for seven bundles and stoichiometry RbC_8. Right is for neutrons and left for x rays.

occupation sites. As the purpose of the calculation is to show the influence of Rb insertion on the diffraction pattern in a first step we artificially fix the same stoichiometry RbC_8 in all the considered cases by playing on the scattering factor of the rubidium. Taking the T site as an example the highest Rb content is RbC_{66}, which is very small. To simulate the case of RbC_8 we multiply the scattering factor of Rb by 66/8. The following parameters are used: mean tube diameter of 13.6 Å and tube-tube distance $a=16.7$ Å. The Rb^+ radius of 2.94 Å taken in this simulation is slightly smaller than in *ab initio* calculation. To avoid interpenetration a minimum Rb^+-C distance of 3.2 Å is assumed.

B. Results

All the curves $I(Q)$ showing the results of model calculations can be directly and quantitatively compared as they correspond to the same stoichiometry. The different $I(Q)$ curves calculated for neutron-diffraction display only small differences (Fig. 6—right panel). The (10) peak around 0.46 $Å^{-1}$ displays a slight downshift for insertion in the surface grooves of the bundles (GS). Its intensity shows a minor increase for triangular site intercalation (T) and decreases equivalently for inner tube volume filling (I sites). More dramatic changes in the diffraction patterns are observed in the case of x-ray scattering (Fig. 6—left panel). Filling the triangular channels (T) produces a strong increase in the (10) peak compared to the raw sample. Inversely, this peak almost disappears when the Rb atoms occupy the interior volume of the tubes (I). This behavior is well known for SWNTs, as it has been explained by different authors.[27–29] One also observes a strong shift of the (10) peak position to small Q for filling of the I sites. A downshift of the (10) reflection accompanied by a decrease in its intensity has been observed in the experimental data (Fig. 2) so that the I site is a good potential candidate as Rb insertion site. The two other cases, i.e., external grooves (GS) and bundle surface (S) display an unexpected behavior. New bumps appear around 0.25 $Å^{-1}$ in the two cases. As these bumps lye in the Q range below 0.45 $Å^{-1}$, it is important to understand their origin.

The simulation of the x-ray diffraction pattern of only one bundle covered by a Rb layer on its external surface is shown in Fig. 7 (left panel, top curve). In the same figure (left panel) the patterns of the bundle alone (middle curve) and of the Rb layer alone (bottom curve) are also shown. The ring of Rb alone displays a diagram with diffraction feet at 0.12, 0.23, 0.33, and 0.43 $Å^{-1}$, the two first ones being rather strong. The same behavior occurs for the bundle alone with a first foot around 0.16 $Å^{-1}$ but with a smaller intensity. The (10) reflection at 0.45 $Å^{-1}$ is not a "foot" but a reflection of the tubes array 2D crystal. When these two objects are coupled (top curve) strong feet is found again but now with different positions compared to the bottom curve. Moreover the (10) reflection is shifted toward small Q. This coupling of the tubes array diffraction pattern with the diffraction pattern of the ring of Rb produces the supplementary bumps in Fig. 6 for S and GS sites. This could be called a "ring effect." The coupling is efficient because the size of the object—the bundle—is nanometric. In the case of very large bundles (~100 tubes) such effect would be negligible as the feet would be at too small Q values. This ring effect for the other sites is small compared to the S and GS sites (see Fig. 7—right panel).

To understand the real impact of this ring effect on the diffraction pattern, a new set of 17 bundles ranging from 3 to 19 tubes with a one tube step from one bundle to the next, was used for calculation. To save time the diameter averaging of $I(Q)$ was not applied. The $I(Q)$ curves for I, T, and GT sites do not change significantly. On contrary the patterns for the S and GS sites change appreciably. As demonstrated in Sec. IV the only sites compatible with a RbC_8 saturation stoichiometry are the I and S sites if one takes account that there is no bundle dilatation. So in the following only these two sites will be considered. The patterns calculated for the I site using the 17 bundles set are given in Fig. 8 (right). According to the results of Sec. IV, the Rb atoms are expected to form a layer very close to the interior surface of the tubes. The two curves correspond to the RbC_8 and $RbC_{4.7}$ (saturated) stoichiometries. A peak appears around 0.72 $Å^{-1}$. On the left-hand side of Fig. 8 are shown the changes in the

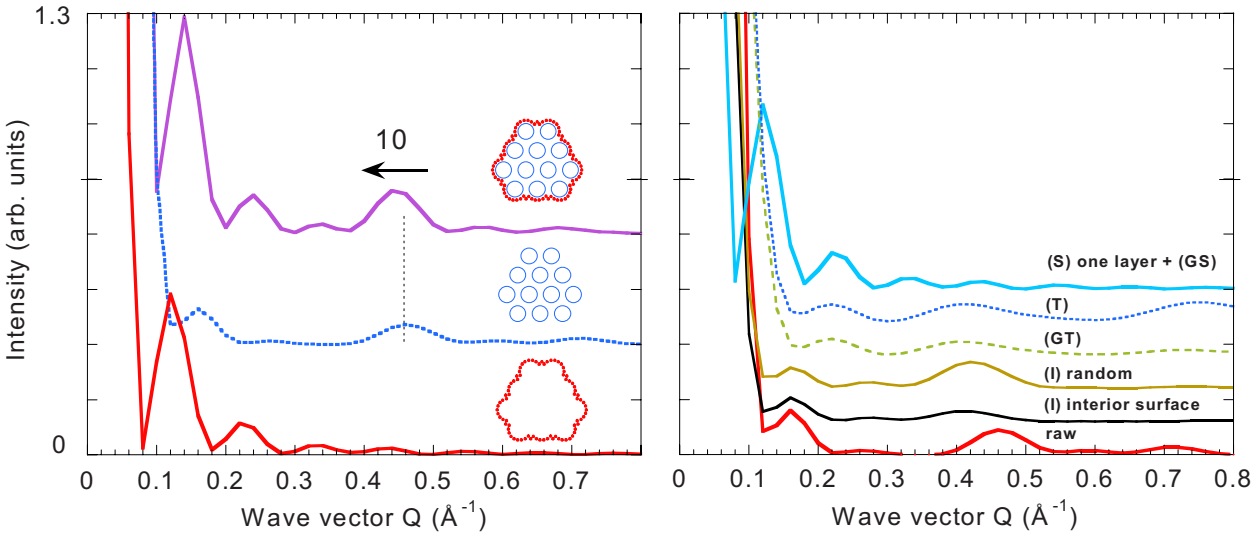

FIG. 7. (Color online) Ring effect. Left: patterns for only one bundle. Right: patterns for the different sites and for the same bundle (Rb only). All curves (left and right) are simulated for x rays.

x-ray pattern for different coverages of the bundle surface. A progressive coverage of the S site with one, two, three, and four layers produces a continuous downshift of the (10) reflection. Moreover a new bump appears around 0.3 Å^{-1} (see the two layers curve) separated from the (10) reflection by a depression. This behavior of the pattern is governed by the ring effect. The depression corresponds to the first zero of the Bessel function that represents the form factor of the tube with the mean diameter. As previously explained, no diameter distribution was taken into account for these latter simulations with 17 bundles. In contrast for a wide diameter distribution this depression would become less pronounced and then the "(10) reflection" would appear with a wide low Q tail as in experimental curves.

VI. DISCUSSION AND CONCLUSION

A sketch of the RbC_8 phase in intercalated graphite is shown in Fig. 9. The Rb atoms open a gap between the graphite planes and occupy positions which face the carbon hexagons. The Rb planes are *intercalated* between two graphite planes. The geometry of SWNT bundles is very different compared to graphite. However an intercalation mechanism can arise if the intertube space is increased. This has been found in SWNT by Duclaux *et al.*[22] with the same stoichiometry compound KC_8. These authors indicate the T site as the most probable occupation site. In their case the vapor phase doping is followed by a long heating treatment which presumably favors the penetration of the potassium atoms inside the bundles and the dilatation of the hexagonal lattice.

The whole analysis of our data (experimental and simulated) suggests instead only two possible sites: the interior of the tubes (I) and the filling of the bundle surface sites (S). According to the energetic criteria the second option is the most favorable, and this hypothesis is supported by the inspection of our calculated diffraction patterns. In fact, they suggest that in the case of I-site intercalation, a new peak on the right-hand side of the (10) reflection should appear around 0.72 Å^{-1}, in contrast with experimental data. More-

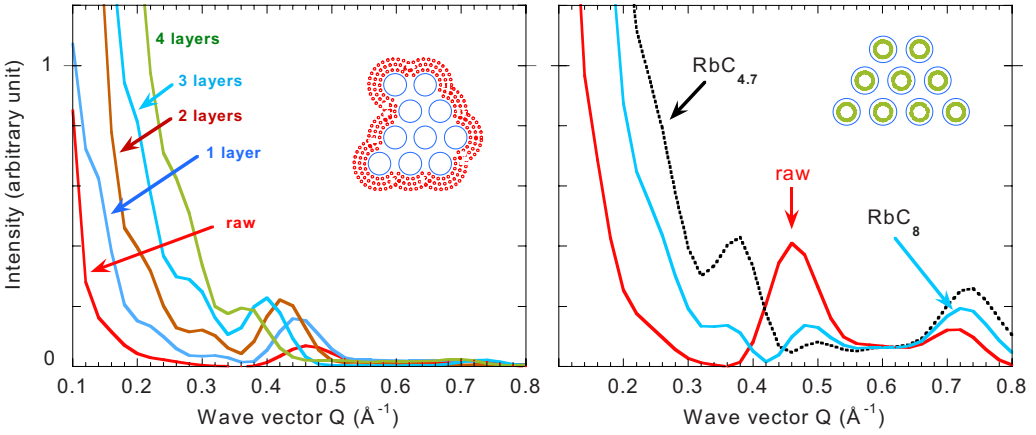

FIG. 8. (Color online) Left: simulated $I(Q)$ for the (S) site with different layers on the bundle surface (x-rays). Right: simulated $I(Q)$ for the interior site (I) with different stoichiometries (x-rays).

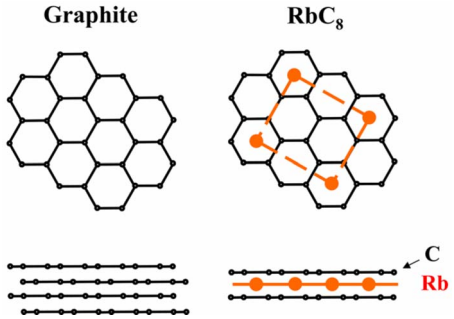

FIG. 9. (Color online) Rb intercalation in graphite stoichiometry RbC_8.

over, in order to penetrate the interior of the tubes, the Rb atoms should first penetrate into the bundles from their surface, which would probably occur by occupying the free space between tubes. *Ab initio* calculations show that the T sites are the most energetically favorable to Rb insertion at small stoichiometry. As a consequence, the intercalants would very unlikely move from their favored T or GT sites to cross high potential barriers and penetrate the tube walls to finally occupy an energetically less favorable site. Moreover, since our samples have never undergone any chemical or physical treatment, the SWNT used for neutrons and x-ray measurements in this work should be closed ends (as synthesized SWNT powder), the Rb ions having thus no easy path to penetrate inside the tubes. On the other hand, the diffraction simulations in Sec. V showed that the spectra corresponding to the interstitial sites strongly disagree with the experimental x-ray diffraction patterns. Our results are very similar to those reported for Ar adsorption on SWNT bundles.[30] At high Ar coverage it was found a significant shift of the (10) peak toward small Q wave vectors. The authors concluded that Ar atoms adsorbed at the outer bundle surface. However the adsorption energy of an Ar atom is much weaker than the insertion energy of a Rb in a SWNT bundle.

In conclusion of the present study of Rb insertion, the most likely intercalation sites are the surface sites. Our combined experimental and theoretical study indicates that the usually observed shift of the lattice (10) peak in x-ray diffraction of rubidium-intercalated SWNT bundles is not due to lattice expansion. As a consequence, the interstitial sites are not the most likely intercalation sites, as previously believed. On the contrary, our work suggests that the bundle surface or, in the case of high-temperature annealing longer than the present case, the inner sites are the most probable ones, and the only ones compatible with x-ray, neutron, *ab initio* calculations, and diffraction simulations.

ACKNOWLEDGMENTS

Calculations in this work have been done at the IDRIS French Computational Facility under Projects No. CP9-51387, No. CP9-61387, and No. CP9-71387 using the QUANTUM-ESPRESSO package.[24]

*nedjma.bendiab@grenoble.cnrs.fr

[1] R. S. Lee, H. J. Kim, J. E. Fischer, A. Thess, and R. E. Smalley, Nature **388**, 255 (1997).
[2] S. Kazaoui, N. Minami, R. Jacquemin, H. Kataura, and Y. Achiba, Phys. Rev. B **60**, 13339 (1999).
[3] A. M. Rao, P. C. Eklund, S. Bandow, A. Thess, and R. E. Smalley, Nature **388**, 257 (1997).
[4] P. Petit, C. Mathis, C. Journet, and P. Bernier, Chem. Phys. Lett. **305**, 370 (1999).
[5] N. Bendiab, L. Spina, A. Zahab, P. Poncharal, C. Marliere, J.-L. Bantignies, E. Anglaret, and J. L. Sauvajol, Phys. Rev. B **63**, 153407 (2001).
[6] N. Bendiab, E. Anglaret, J.-L. Bantignies, A. Zahab, J. L. Sauvajol, P. Petit, C. Mathis, and S. Lefrant, Phys. Rev. B **64**, 245424 (2001).
[7] N. Bendiab, A. Righi, E. Anglaret, J. Sauvajol, L. Duclaux, and F. Beguin, Chem. Phys. Lett. **339**, 305 (2001).
[8] N. Bendiab, Ph.D. thesis, Université Montpellier II, 2003.
[9] X. Liu, T. Pichler, M. Knupfer, and J. Fink, Phys. Rev. B **67**, 125403 (2003).
[10] J. T. Ye, Z. M. Li, Z. K. Tang, and R. Saito, Phys. Rev. B **67**, 113404 (2003).
[11] G. Chen, C. A. Furtado, U. J. Kim, and P. C. Eklund, Phys. Rev. B **72**, 155406 (2005).
[12] H. Rauf, T. Pichler, M. Knupfer, J. Fink, and H. Kataura, Phys. Rev. Lett. **93**, 096805 (2004).
[13] B. Akdim, X. Duan, D. A. Shiffler, and R. Pachter, Phys. Rev. B **72**, 121402(R) (2005).
[14] P. Corio, A. Jorio, N. Demir, and M. S. Dressalhaus, Chem. Phys. Lett. **392**, 396 (2004).
[15] S. B. Cronin, R. Barnett, M. Tinkham, S. G. Chou, O. Rabin, M. S. Dresselhaus, A. K. Swan, M. S. Unlu, and B. B. Goldberg, Appl. Phys. Lett. **84**, 2052 (2004).
[16] Z. Wang, H. Pedrosa, T. Krauss, and L. Rothberg, Phys. Rev. Lett. **96**, 047403 (2006).
[17] N. Caudal, A. M. Saitta, M. Lazzeri, and F. Mauri, Phys. Rev. B **75**, 115423 (2007).
[18] A. Das, A. K. Sood, A. Govindaraj, A. M. Saitta, M. Lazzeri, F. Mauri, and C. N. R. Rao, Phys. Rev. Lett. **99**, 136803 (2007).
[19] A. Thess, R. Lee, P. Nikolaev, H. J. Dai, P. Petit, J. Robert, C. H. Xu, Y. H. Lee, S. G. Kim, A. G. Rinzler, D. T. Colbert, G. E. Scuseria, D. Tomanek, J. E. Fischer, and R. E. Smalley, Science **273**, 483 (1996).
[20] S. Rols, R. Almairac, L. Henrard, E. Anglaret, and J.-L. Sauvajol, Eur. Phys. J. B **10**, 263 (1999).
[21] N. Bendiab, R. Almairac, S. Rols, R. Aznar, J.-L. Sauvajol, and I. Mirebeau, Phys. Rev. B **69**, 195415 (2004).
[22] L. Duclaux, J. P. Salvetat, P. Lauginie, T. Cacciaguera, A. M. Faugre, C. Goze-Bac, and P. Bernier, J. Phys. Chem. Solids **64**, 571 (2003).
[23] V. Meunier, J. Kephart, C. Roland, and J. Bernholc, Phys. Rev. Lett. **88**, 075506 (2002).

[24] S. Baroni *et al.*, www.quantum-espresso.org
[25] J.-L. Bantignies, L. Alvarez, R. Aznar, R. Almairac, J.-L. Sauvajol, L. Duclaux, and F. Villain, Phys. Rev. B **71**, 195419 (2005).
[26] J. Lu, S. Nagase, S. Zhang, and L. Peng, Phys. Rev. B **69**, 205304 (2004).
[27] A. Fujiwara, K. Ishii, H. Suematsu, H. Kataura, Y. Maniwa, S. Suzuki, and Y. Achiba, Chem. Phys. Lett. **336**, 205 (2001).
[28] J. Cambedouzou, V. Pichot, S. Rols, P. Launois, P. Petit, R. Klement, H. Kataura, and R. Almairac, Eur. Phys. J. B **42**, 31 (2004).
[29] W. Zhou, K. I. Winey, J. E. Fischer, T. V. Streekumar, S. Kumar, and H. Kataura, Appl. Phys. Lett. **84**, 2172 (2004).
[30] M. Bienfait, P. Zeppenfeld, N. Dupont-Pavlovsky, J.-P. Palmari, M. R. Johnson, T. Wilson, M. DePies, and O. E. Vilches, Phys. Rev. Lett. **91**, 035503 (2003).